Rock Mechanics and Rock Engineering (2021) 54:1779–1797
https://doi.org/10.1007/s00603-020-02346-2

ORIGINAL PAPER

A Simplified Model for Time-Dependent Deformation of Rock Joints

Mingzheng Wang[1] · **Ming Cai**[1,2,3]

Received: 31 January 2020 / Accepted: 15 December 2020 / Published online: 10 January 2021

Abstract

Understanding the time-dependent deformation behavior of rock joint is important when evaluating long-term stability of structures built on or in jointed rock masses. This study focuses on the time-dependent strength and deformation of unweathered clean rock joints. First, five grain-scale joint models are established based on Barton's standard joint profiles using the GBM-TtoF creep material model. Barton's non-linear shear strength criterion is adopted to determine the short-term shear strength of the joints. Second, a series of creep simulations are conducted to investigate major factors (normal stress, shear loading ratio, and joint roughness) that influence the long-term shear strength and the sliding velocity of the joints. The results reveal that normal stress has more influence than joint roughness on resisting creep slipping of the joints. Third, an equation for the prediction of creep sliding velocity is developed by fitting the simulation results and the equation is verified by experimental data. Finally, a creep slipping model for simplified flat joints is proposed, which can be used to model the long-term shear strength and sliding velocity of joints under creep deformation conditions. The creep slipping model, which can be used in both stationary and variable stress conditions, is useful for simulating time-dependent behaviors of jointed rock mass using the distinct element method.

Keywords Time-dependent behavior · Rock joints · Grain-based model · Creep model of joint · GBM-UDEC

List of Symbols

τ_S	Short-term shear strength
τ_L	Long-term shear strength
JCS	Joint wall compressive strength
ϕ_b	Basic friction angle of macro-joint
JRC	Joint roughness coefficient
σ_n	Normal stress
UCS	Uniaxial compressive strength of rock
c	Cohesion of rock in the TtoF (time-to-failure) model
ϕ	Friction angle of rock in the TtoF model
σ_t	Tensile strength of rock in the TtoF model
c^c	Cohesion of contact element
ϕ^c	Friction angle of contact element
σ_t^c	Tensile strength of contact element
i	Dilation angle of contact element
Jks	Shear stiffness of contact element
Jkn	Normal stiffness of contact element
τ/τ_S	Shear loading ratio
ξ	Long-term shear strength ratio
JRC_{mob}	Mobilized joint roughness
ϕ_{mob}	Mobilized joint friction angle
JRC_{c-mob}	Mobilized joint roughness due to creep damage
C_j	Dimensionless parameter
ξ_0	Basic long-term shear strength ratio

✉ Ming Cai
mcai@laurentian.ca

Mingzheng Wang
mwang3@laurentian.ca

[1] Bharti School of Engineering, Laurentian University, Sudbury, ON, Canada

[2] MIRARCO-Mining Innovation, Laurentian University, Sudbury, ON, Canada

[3] Key Laboratory of Ministry of Education for Safe Mining of Deep Metal Mines, Northeastern University, Shenyang, China

1 Introduction

Many important issues in rock mechanics and rock engineering are related to the presence of fractures in rocks (Kemeny 2003). This is especially true for brittle rocks because joints usually have a weaker strength and can experience larger displacements (Barton 1995; Bhasin and Høeg 1998; Boon 2013; Wasantha et al. 2015). Many field evidences show that the mechanical behavior of rock joints in brittle rock mass should be considered time-dependent. This is important for geotechnical structures with a long service life, such as civil tunnels (Bieniawski 1976, 1989; Cristescu et al. 1987), high slopes (Chigira 1992; Feng et al. 2003; Xu et al. 2013), and nuclear waste disposal repositories (Martín et al. 2015; Shrader-Frechette 1993). For these structures built in jointed rock masses, their stability is often governed by the time-dependent deformation of joints (Glamheden and Hoekmark 2010; Liu et al. 2004). Thus, time-dependent strength and deformation of rock joints is an important issue that needs to be addressed in rock engineering design.

Lajtai (1991, 1989) found that the peak shear strength of joints of Lac du Bonnet (LdB) granite with smooth joint walls, which is called short-term shear strength τ_S in our study, is time-dependent. Under constant normal and shear stress loadings, the friction angle of the joints increased about 4° after a delayed time of 2 to 3 days. The stress–displacement relation returned to the pre-delayed position after such additional frictional resistance was overcome. This time-strengthening phenomenon may result from the gradual increase of the contact area of the joint surface due to the creep deformation of micro-asperities (Malan 1998). However, as Lajtai (1989) mentioned, such a time-strengthening phenomenon is hard to predict because it is loading-rate dependent. Thus, this additional frictional strength increase is not considered in this study.

The long-term shear strength of joints, which is noted as τ_L in this article, has been studied by some scholars in laboratory using different types naturally occurring and artificially made rock joints (He et al. 2019; Malan 1998; Shen and Zhang 2010; Yang et al. 2007; Zhang et al. 2012, 2015) and artificial joints made using concrete (Wang et al. 2017a, 2016; Zhang et al. 2019). Wang (2017b) used Goodman's creep model of intact rock (Goodman 1989) to describe the long-term shear strength of joints. When the shear stress of a joint is lower than its long-term shear strength, the creep deformation will stop when the shear stress reaches the creep terminal locus (Fig. 1). If the shear stress is higher than the long-term shear strength of the joint, the creep deformation will continue until failure of the joint occurs.

Burgers model, which can describe the initial and secondary creep deformation stages, is widely used to fit creep strain curves of rock and joint obtained from experiments (Xu and Yang 2005; Yang et al. 2007, 2013; Zhang et al. 2012, 2016). Normal stress, roughness and shear stress can influence the four model parameters of Burgers model; however, it is unclear how these model parameters are influenced for joints, which is the subject of the study of this paper.

As Lajtai (1989) stated, it is hard to obtain representative samples to conduct creep tests using natural joints because the mechanical properties of joints tend to be more variable than intact rock. In addition, conducting a shear creep test of joint is very time consuming. As a result, available experimental data from published literature are limited.

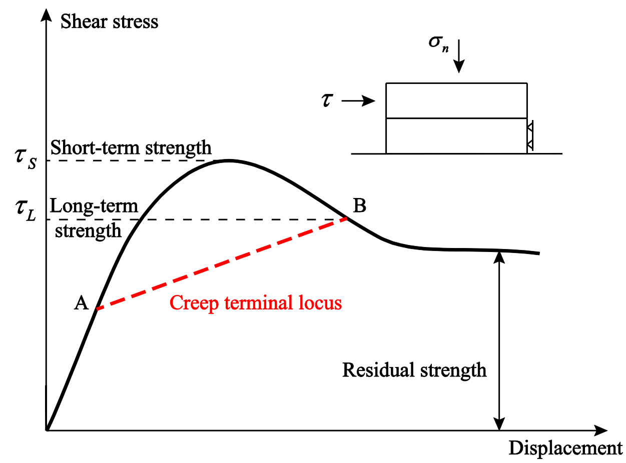

Fig. 1 Time-dependent strength of rock joint, after Glamheden (2010) and Wang et al. (2017b)

There are a few studies that focus on numerical simulation of time-dependent deformation behaviors of rock joint (Chen et al. 2004; Xu et al. 2013; Xue and Mishra 2019). When modeling time-dependent deformation behavior of jointed rock mass using DEM (distinct element method) software such as UDEC (Itasca 2015), time-dependent displacements of joints should be considered. However, there is no creep constitutive model for rock joints in UDEC, which limits its applications. On the other hand, it has been found that micro-scale models can simulate time-dependent deformation behaviors of intact rock well using the strength degradation method (Liu and Cai 2020; Potyondy 2007; Wang and Cai 2020; Zhang and Wong 2013). Damage initiation and crack propagation under the creep loading condition can be captured at the grain scale. When a rock joint model is built using a micro-scale model, the mechanical behavior of the rock of the joint walls can be considered time-dependent. As a result, time-dependent deformation behaviors of rock joint can be simulated by simulating time-dependent deformations of intact rock. In this way, the damage of joint wall asperities under creep loading conditions can be investigated at the grain-scale level. The grain-based time-to-failure model (GBM-TtoF) by Wang and Cai (2020) is a grain-scale creep model that can simulate time-dependent deformation behaviors of brittle rocks, and this model is used to investigate time-dependent deformations of rock joints in this study.

This article presents a study of the creep mechanism of brittle rock joints under shear loading. Firstly, grain-scale joint models are established to mimic the creep deformation of rock joints. Then, some major factors that influence the creep deformation of rock joints, such as normal stress, shear stress and joint roughness, are investigated numerically using the grain-scale joint models. Finally, a new strength degradation creep model for joints is introduced, which can be used to model time-dependent strength and deformation of flat joints in UDEC for engineering applications. A flowchart is presented in Fig. 2 to illustrate the procedure of this study for the development of the joint creep slipping model.

2 Grain-Scale Model Implementation

When investigating the mechanical responses of joint by numerical simulation, the meso-scale modeling method, which can establish the micro-structures of joint roughness, can be used to build joint models. Existing constitutive models of intact rock can be used to model the strength and time-dependent deformation of intact rock. In this way, the deformation and damage that occur on the joint asperities can be captured (Bahaaddini et al. 2016). The resulting deformation behavior of the model represents the behavior of a rock joint.

According to the Barton's shear strength criterion of rock joints (Bandis et al. 1981; Barton et al. 1985), the joint roughness and the joint wall compressive strength (*JCS*) are two important factors that influence the short-term shear strength of unweathered clean rock joints. For joints under creep loading, time-dependent deformations of asperities also influence the long-term strength and deformation of joints (Wang et al. 2015; Zhang et al. 2019). Thus, five joint models with realistic joint profiles are established in UDEC to represent the geometry of joint asperities, as shown in Fig. 3a, b.

The rock of the joint walls are modeled using the GBM-TtoF model proposed by Wang and Cai (2020), and an enlarged view of the joint walls is shown in Fig. 3c. The GBM-TtoF model is a grain-scale creep model that can be

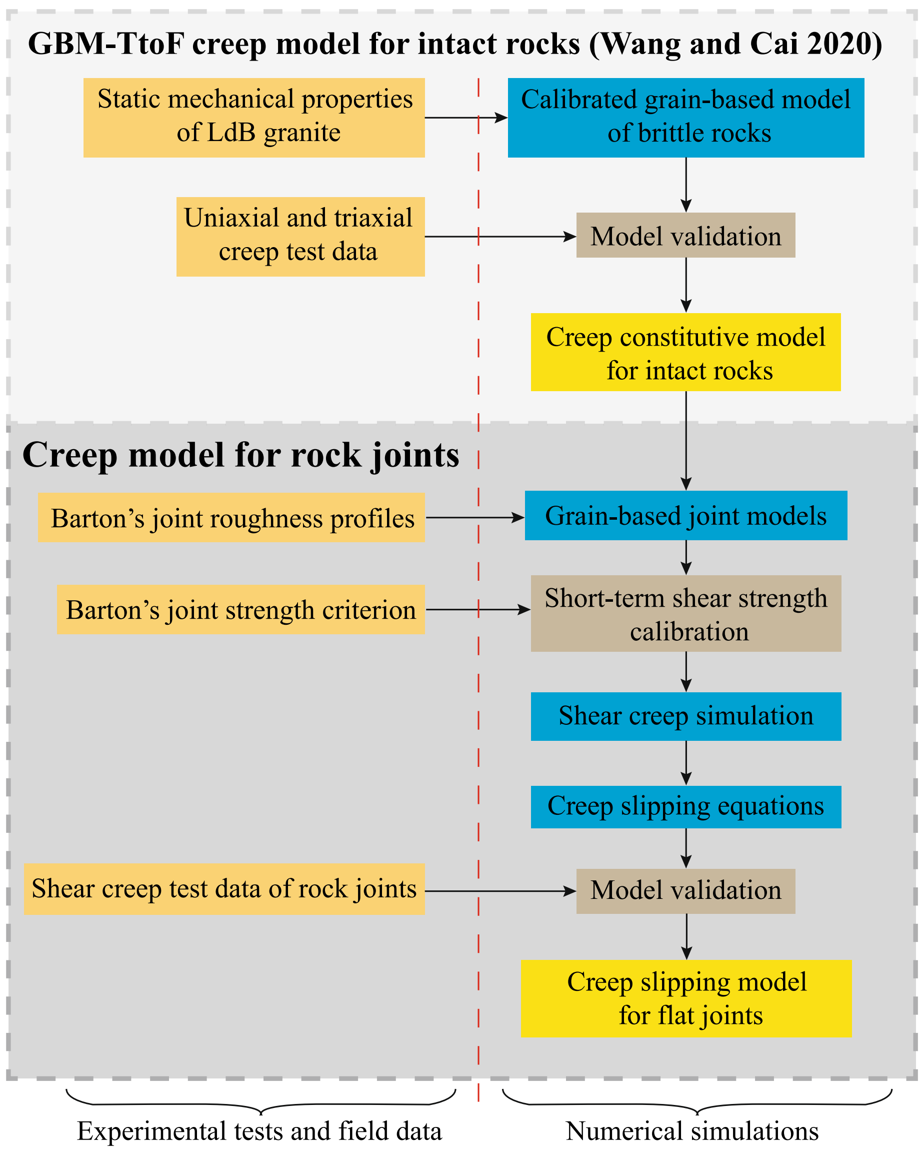

Fig. 2 Flowchart of the joint creep slipping model development

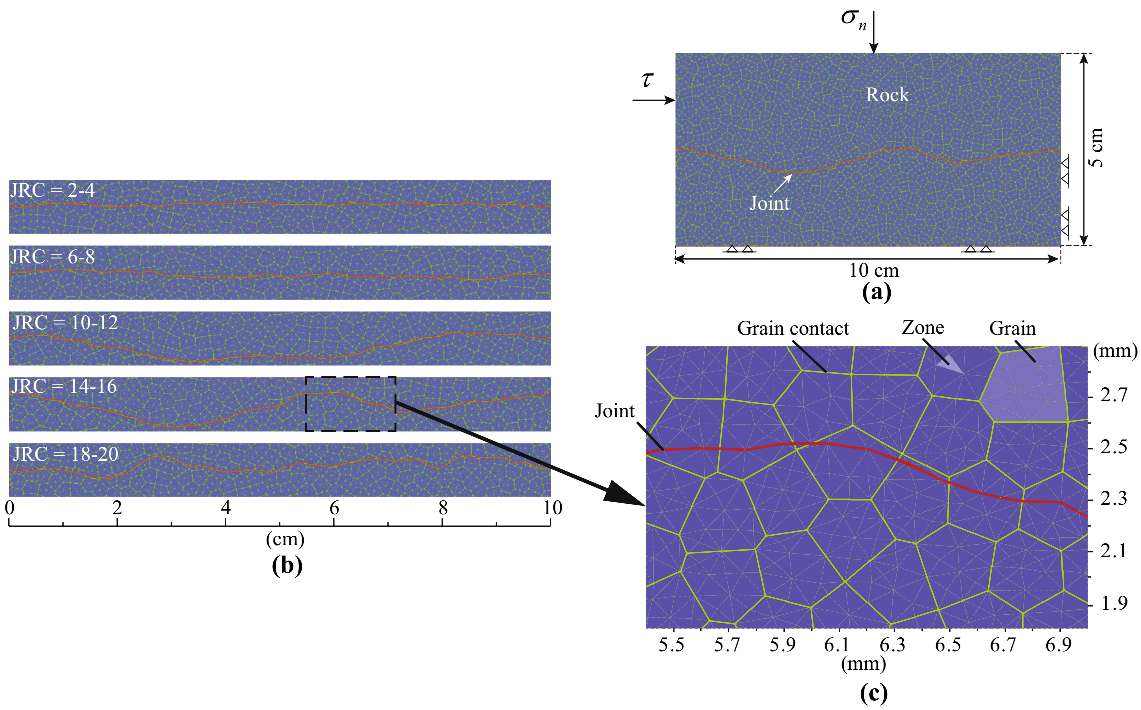

Fig. 3 (**a**) Shear model of joint implemented in UDEC; (**b**) five grain-scale joint models based on Barton's standard joint profiles; (**c**) enlarged view of microstructure of asperities along the joint surface for $JRC = 14$–16

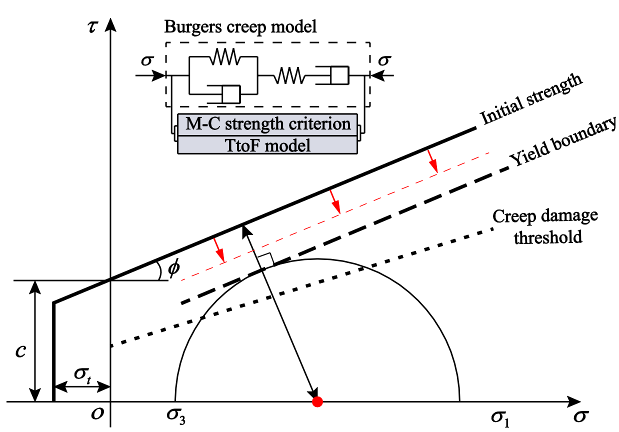

Fig. 4 GBM-TtoF creep model (Wang and Cai 2020)

used to simulate creep deformations of brittle rocks. Gradual damage of grains and contacts due to stress corrosion under creep loading can be simulated. In the GBM-TtoF model, Burgers model is used to model creep deformations of grains. The short-term strength of grains is assumed to follow the Mohr–Coulomb (M–C) failure criterion, and the long-term strength is assumed equal to the crack damage strength of rock. When a rock is loaded beyond the long-term strength, the strengths of grains and contacts degrade in the manner as illustrated in Fig. 4. The degradation parameters are calibrated using laboratory static fatigue test data.

The creep deformation and failure of joints with joint asperities are governed by the creep model of rock, i.e., the GBM-TtoF model. In this manner, the time-dependent deformation behavior of joints is controlled by the mechanical response of grains and the geometry of grains representing the joint asperities. Sliding and static fatigue of joint asperities can be presented at the grain-scale level in the simulation.

The micro-parameters of the GBM-TtoF models are calibrated using static fatigue experimental data of LdB granite by Wang and Cai (2020). As mentioned above, Barton's standard joint roughness profiles (Barton and Choubey 1977) are adopted to build surface waviness of the joints in the grain-scale joint models. The length of the contact elements of joint is defined as small as possible. In our simulation, we used the length of 1.5e-3 m, which equals to the average size of the zones in the grains of the GBM-TtoF model (Fig. 3c).

3 Short-Term Shear Strength Calibration

According to the Barton's non-liner shear strength model of rock joints, there is no cohesion between clean joint walls. The friction angle of an unweathered rock joint consists of two parts (Eq. (1)): one is the basic friction angle ϕ_b, which is determined by the friction angle of saw-cut smooth joint walls; the other is the dilation angle, which is influenced by normal stress σ_n, *JCS* and *JRC* (joint roughness coefficient). For unweathered fresh joints of LdB granite, the basic friction angle ϕ_b is equal to $30° \pm 2°$ (Alejano et al. 2012; Barton et al. 1985) and the *JCS* is equal to the uniaxial compressive strength (*UCS*) of 225 MPa (Schmidtke and Lajtai 1985; Wang and Cai 2020). The mechanical parameters of the grain-scale joint model are calibrated according to the Barton's strength criterion shown below:

$$\tau_S = \sigma_n \tan\left[JRC \log\left(\frac{JCS}{\sigma_n}\right) + \phi_b\right], \tag{1}$$

where the τ_S is the short-term shear strength of joint and *JCS* is the joint wall compressive strength.

As shown in Fig. 3c, the macro-joint in the grain-scale joint model has many contact elements, the strength of which is assumed to follow the Mohr–Coulomb strength criterion. There are six mechanical parameters for the contact elements, which are cohesion c^c, friction angle ϕ^c (ϕ^c is a micro-parameter which is not the basic friction angle ϕ_b of the macro-joint), tensile strength σ_t^c, dilation angle i, shear stiffness Jks, and normal stiffness Jkn. Because a joint has no cohesion, c^c and σ_t^c are equal to zero. Because the grain-scale joint models are established using actual joint roughness profiles, dilation in the normal direction during shear deformation is driven by the waviness of the joint walls. Hence, the dilation angle of the joint element i is equal to zero. The initial values of Jks and Jkn are equal to those of the contacts of the grains. The initial value of the friction angle ϕ^c is equal to 30°.

According to the results of a parameter study we conducted, it is seen that both Jks and ϕ^c influence the short-term shear strength of joint, the degree of which is governed by the joint roughness. Figure 5 presents the results for two joints with different roughness ($JRC = 0$ and 7) under a normal stress of 2 MPa. The short-term strength increases as Jks increases. For these two models, the friction angle of

Fig. 5 Influence of *Jks* on the short-term shear strength of joints with different roughness

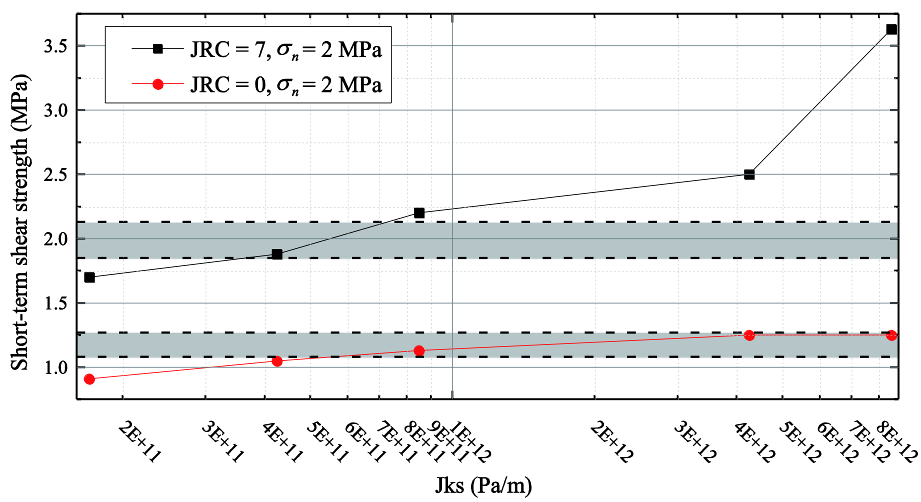

Fig. 6 Influence of friction angle of contact elements on the short-term shear strength of flat joints

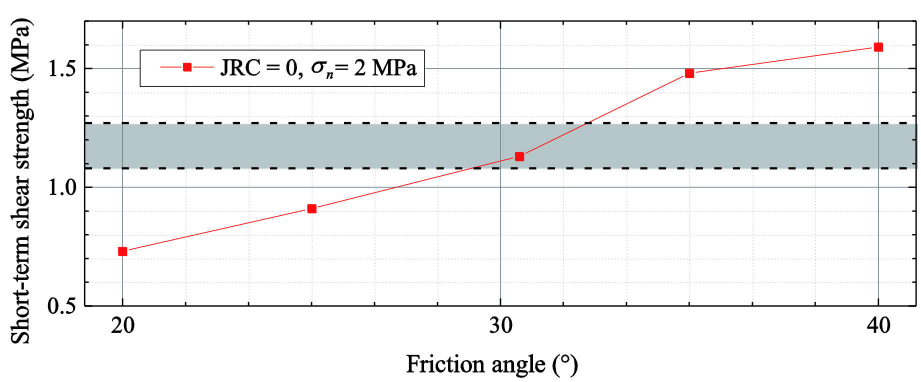

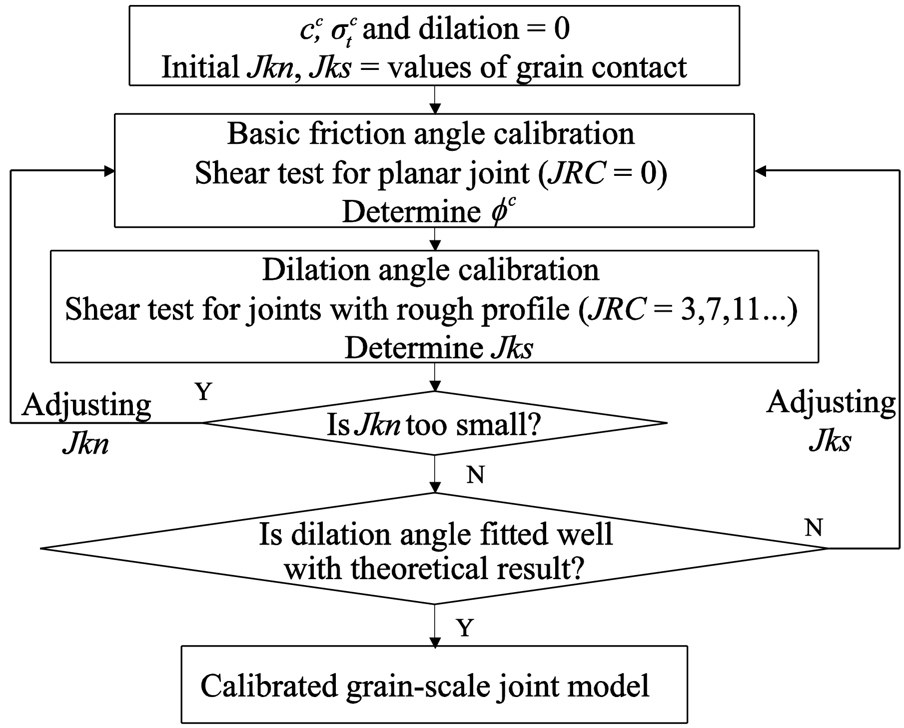

Fig. 7 Flowchart showing the short-term shear strength calibration process

the joint contact elements ϕ^c is 30.5°. Figure 6 shows the influence of contact friction angle ϕ^c on the short-term shear strength of flat joints ($JRC=0$) with $Jks=8.5e11$ Pa/m. The gray region indicates the shear strengths calculated from Eq. (1) with the basic friction angle $\phi_b=30°\pm2°$. As illustrated in these two figures, the friction angle ϕ^c is the key parameter that controls the shear strength of a flat joint ($JRC=0$). For a rough joint ($JRC=7$), both ϕ^c and *Jks* influence the shear strength of the joint.

The final values of *Jks*, *Jkn* and ϕ^c are determined following the process shown in Fig. 7. First, the fiction angle ϕ^c is determined by the shear test simulation using a flat joint model ($JRC=0$). Then, the *Jks* values are determined by shear test simulations using the rough joint models ($JRC=3$, 7, 11, …). A few iterations are necessary to obtain satisfactory results.

The calibrated shear strengths of the five joint models are presented in Fig. 8, which agree well with the strengths defined by Barton's model. In the simulation models, the fitted basic friction angle of LdB granite is 30.5°. The parameters of the contact elements of the joints are summarized in Table 1.

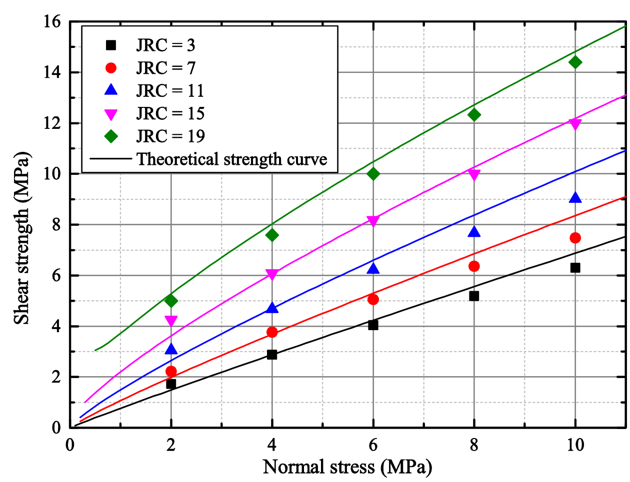

Fig. 8 Calibrated results of short-term shear strength of five joint models with different roughness

Table 1 Calibrated micro-parameters of contact elements of joint

Micro-parameters	Value
Jks(Pa/m)	8.5e11
Jkn(Pa/m)	8.8e14
Friction (°)	30.5
Cohesion (MPa)	0
Tensile strength (MPa)	0
Dilation angle (°)	0

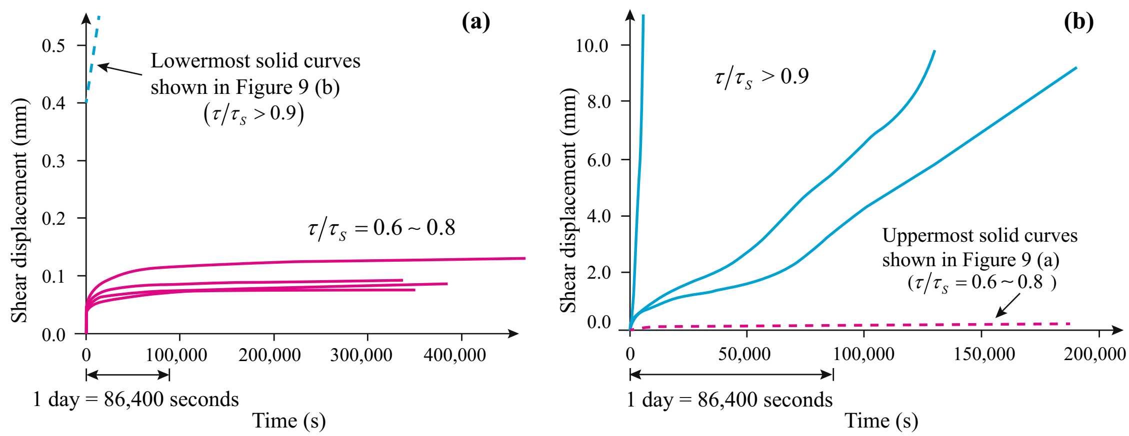

Fig. 9 Creep deformations of joints from experimental tests (Bowden and Curran 1984)

4 Numerical Simulation of Joint Creep Under Shear Loading

4.1 Long-Term Shear Strength

When loaded under constant normal and shear stresses, time-dependent deformation behaviors of joints are different under low and high shear loading ratios τ/τ_S, where τ is the shear stress and τ_S is the short-term shear strength of a joint. According to Bowden and Curran (1984)'s experimental results shown in Fig. 9, the creep deformation will stop eventually if the applied shear stress is below a threshold. If the applied shear stress is beyond the threshold, the joint will keep slipping at a relatively constant speed. If the ratio of the long-term (τ_L) to the short-term (τ_S) shear strengths is referred as the long-term shear strength ratio ξ, defined in Eq. (2), the ξ value is about 0.9 for Bowden and Curran (1984)'s experimental results (Fig. 9).

$$\xi = \frac{\tau_L}{\tau_S}. \tag{2}$$

According to the test results of unfilled rock joints, the long-term shear strength ratio ξ is equal to 0.3 to 0.6 for joints of soft rock (Zhang et al. 2012), 0.7 to 0.9 for joints of brittle hard rock (Bowden and Curran 1984; He et al. 2019). For the same rock type, the long-term shear strength of joints is largely influenced by two factors—joint roughness and normal stress. Currently, it is still not clear how the ξ values are influenced by these two factors. Thus, to improve the understanding of this issue, shear creep simulations are conducted using the five grain-scale joint models (*JRC* = 3, 7, 11, 15 and 19) under different normal stresses (σ_n = 2, 4 and 8 MPa).

Figure 10 presents the simulated creep strain curves of two joints (*JRC* = 3 and 19) under low (σ_n = 2 MPa) and high (σ_n = 8 MPa) normal stresses. It can be seen that the ξ values are equal to 0.850, 0.550, 0.975 and 0.925 for the cases shown in Fig. 10a–d, respectively. The trial and error method is used to determine ξ. When the shear loading ratio τ/τ_S exceeds ξ, the joint slips at a constant velocity. The slipping of a joint will stop if the shear loading ratio τ/τ_S is smaller than ξ. The average of the two shear loading ratios is determined as the long-term shear strength ratio ξ.

The long-term shear strength ratio ξ depends on the normal stress and the *JRC* value. As shown in Fig. 10a, c, for the joint with *JRC* = 3, the ξ value increases from 0.850 to 0.975 when the normal stress increases from 2 to 8 MPa. For the joint with *JRC* = 19, the ξ value increases from 0.550 to 0.925 when the normal stress increases from 2 to 8 MPa. The roughness also influence the ξ value. When the *JRC* values increase from 3 to 19 under the normal stress of 2 MPa, the ξ values decrease from 0.925 to 0.550 (Fig. 10a, b).

It is easy to understand that both the σ_n and *JRC* have a positive correlation with the long-term (τ_L) and short-term (τ_S) shear strengths (Fig. 11). However, the influence of σ_n and *JRC* on the long-term shear strength ratio ξ is complex. Figures 12 and 13 present the simulated results of the five joint models. Figure 12 shows that the long-term shear strength ratio ξ has a positive correlation with σ_n, especially for joints with rough profiles (*JRC* = 15 or 19). The ξ value is more sensitive to the normal stress. On the other hand, ξ tends to have a negative correlation with *JRC*, as illustrated in Fig. 13. Although not very strong, the negative correlation can be observed. For example, ξ increases when *JRC* increase from 7 to 11 for σ_n = 4 MPa. The fluctuations are resulted from the variation of the strength properties of joints due to the randomness of Voronoi grain geometry. The negative correlation between *JRC* and ξ is also observed in the laboratory test results

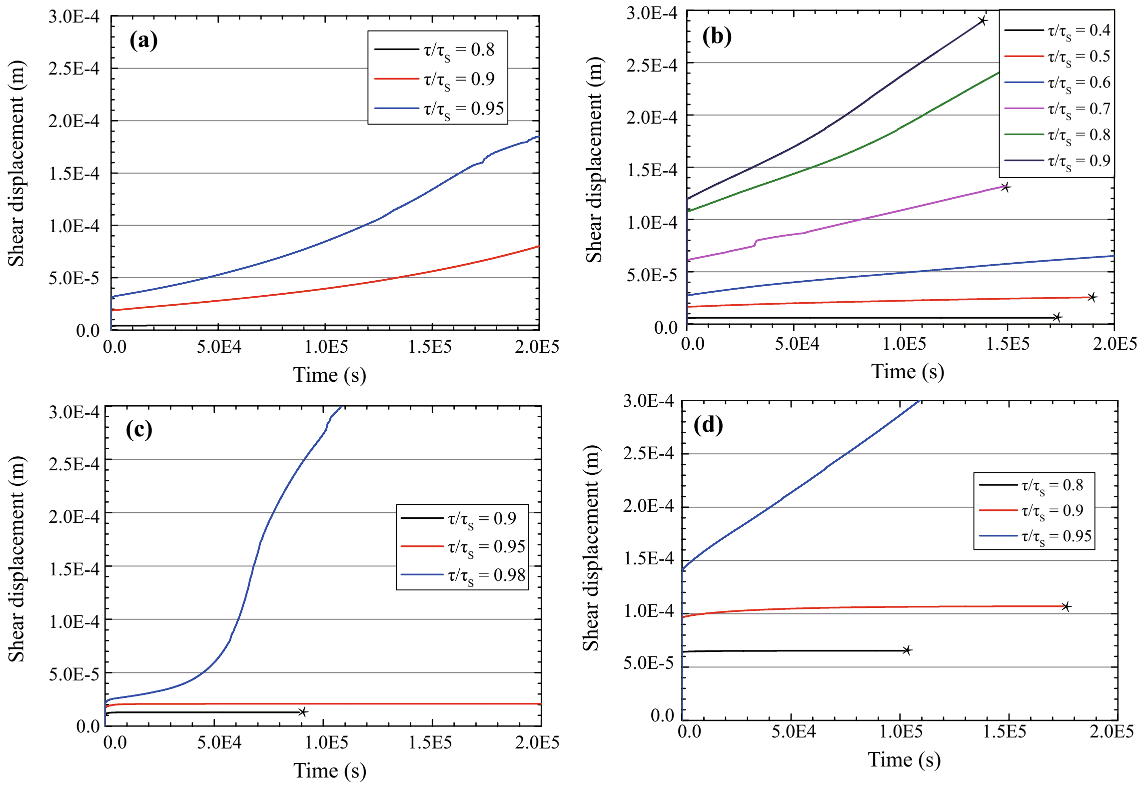

Fig. 10 Simulated creep strain curves of joints under different τ/τ_S ratio: (**a**) joint with $JRC=3$, $\sigma_n=2$ MPa; (**b**) joint with $JRC=19$, $\sigma_n=2$ MPa; (**c**) joint with $JRC=3$, $\sigma_n=8$ MPa; (**d**) joint with $JRC=19$, $\sigma_n=8$ MPa. *Means that the simulation is stopped by user

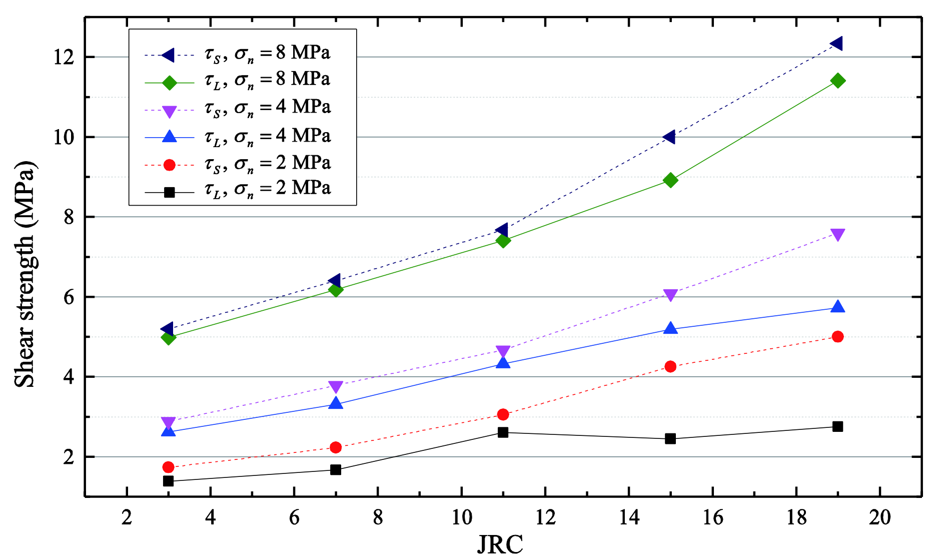

Fig. 11 Influence of *JRC* and σ_n on the long-term shear strength of joint

of Wang et al. (2017b) who used artificial concrete joints in their tests.

The influence of the *JRC* and normal stress on the long-term shear strength ratio ξ of rock joints can be explained using Barton's joint shear strength model to consider what proportion of the shear strength from the joint asperity is used to resist creep slipping. According to Barton's model shown in Fig. 14, after the peak strength is reached in static shear tests, the roughness of joints is lost continuously with the increase of shear displacement. This part of the roughness is called JRC_{mob}, which is approximately 50% of the initial *JRC* when the post-peak shear displacement reaches 10 times of the displacement at the peak strength, i.e.,

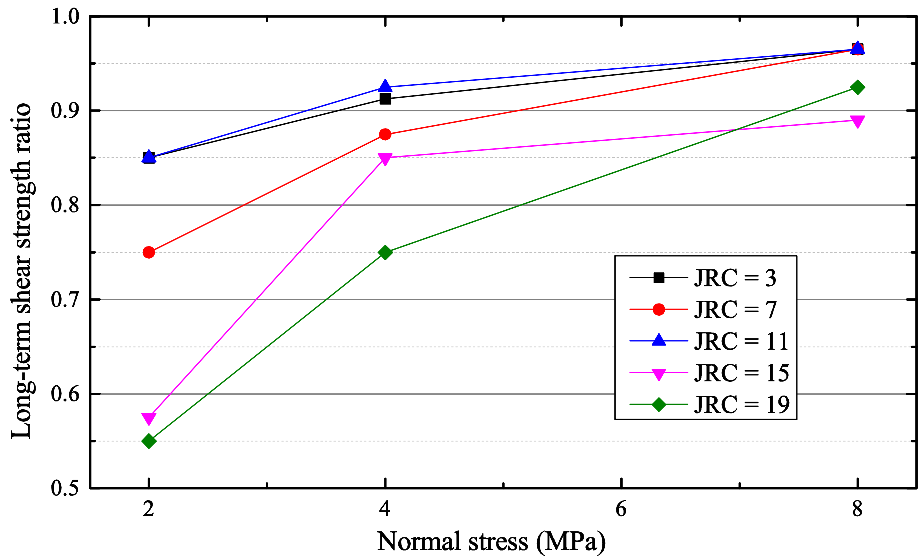

Fig. 12 Influence of σ_n on the long-term shear strength ratio

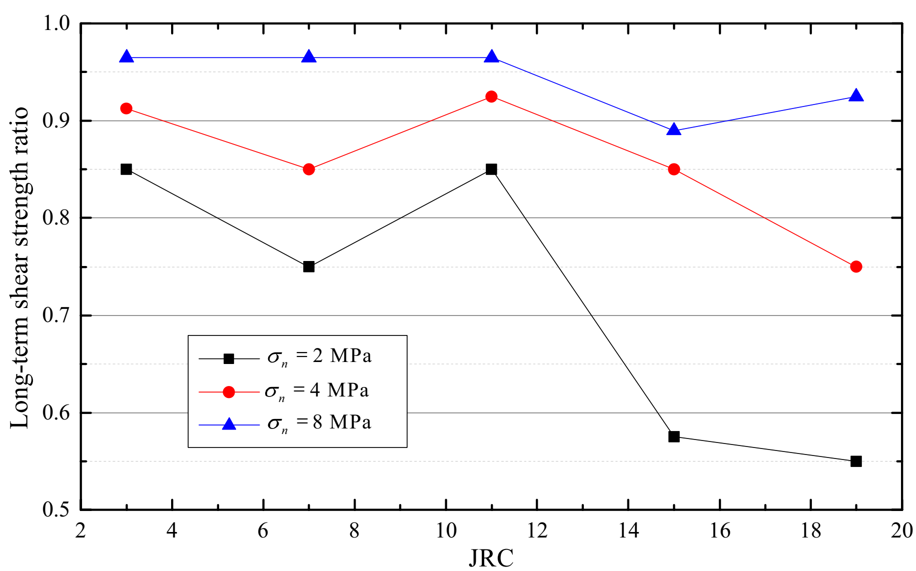

Fig. 13 Influence of *JRC* on the long-term shear strength ratio

$$\frac{JRC_{mob}}{JRC} \approx 0.5. \tag{3}$$

The decrease of the joint friction angle ϕ_{mob} due to the destruction of the roughness can be calculated using

$$\phi_{mob} = JRC_{mob} \log\left(\frac{JCS}{\sigma_n}\right). \tag{4}$$

Similar to that in the static shearing (Fig. 15a), the degradation of joint asperities is also a major form of joint failure in creep deformation, as illustrated in Fig. 15b. The roughness degradation is quite obviously in the simulation using the grain-scale joint models, as illustrated in Fig. 15c, d using the damage index contours to show the strength degradation of grains along the joint surfaces. Thus, it can be assumed that the maximum amount of roughness loss due to creep fatigue is also limited to a proportion of the initial roughness even after a long time, in a similar form as the roughness loss under static loading presented in Eq. (3). Hence, the maximum roughness loss that can occur in the creep fatigue process, JRC_{c-mob}, is assumed to be related to the initial *JRC* as

$$\frac{JRC_{c-mob}}{JRC} \approx cons, \tag{5}$$

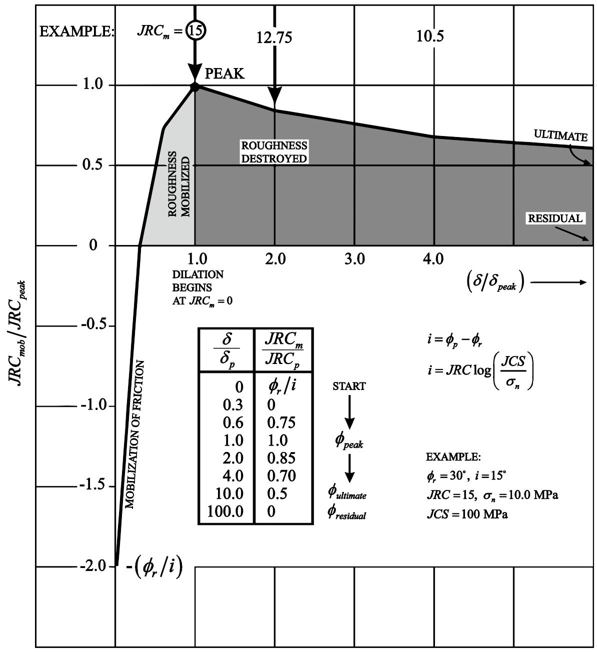

$\frac{\delta}{\delta_p}$	$\frac{JRC_m}{JRC_p}$
0	ϕ_r/i
0.3	0
0.6	0.75
1.0	1.0
2.0	0.85
4.0	0.70
10.0	0.5
100.0	0

Fig. 14 JRC_{mob} concept developed by Barton et al. (1985)

where *cons* is a constant between 0 and 1.

For two joints (Joint I and Joint II) with different initial roughness with

$$JRC^{I} > JRC^{II}, \tag{6}$$

and if they are loaded under the same normal stress, according to Eqs. (1), (2) and (4), the long-term shear strength ratio ξ of Joint I can be calculated by

$$\xi^{I} = \frac{\left(JRC^{I} - JRC^{I}_{c-mob}\right)\log\left(\frac{JCS}{\sigma_n}\right) + \phi_b}{JRC^{I}\log\left(\frac{JCS}{\sigma_n}\right) + \phi_b}, \tag{7}$$

The long-term shear strength ratio ξ^{II} of Joint II can be calculated in the same way. Then according to Eqs. (5), (6) and (7), we have

$$\xi^{I} < \xi^{II}, \tag{8}$$

which means that for a joint with a larger initial *JRC* value, it has a lower long-term shear strength ratio ξ.

The positive correlation between normal stress and ξ can also be explained. For example, if one joint is loaded under different normal stresses, which are denoted as σ_n^{I} and σ_n^{II} with

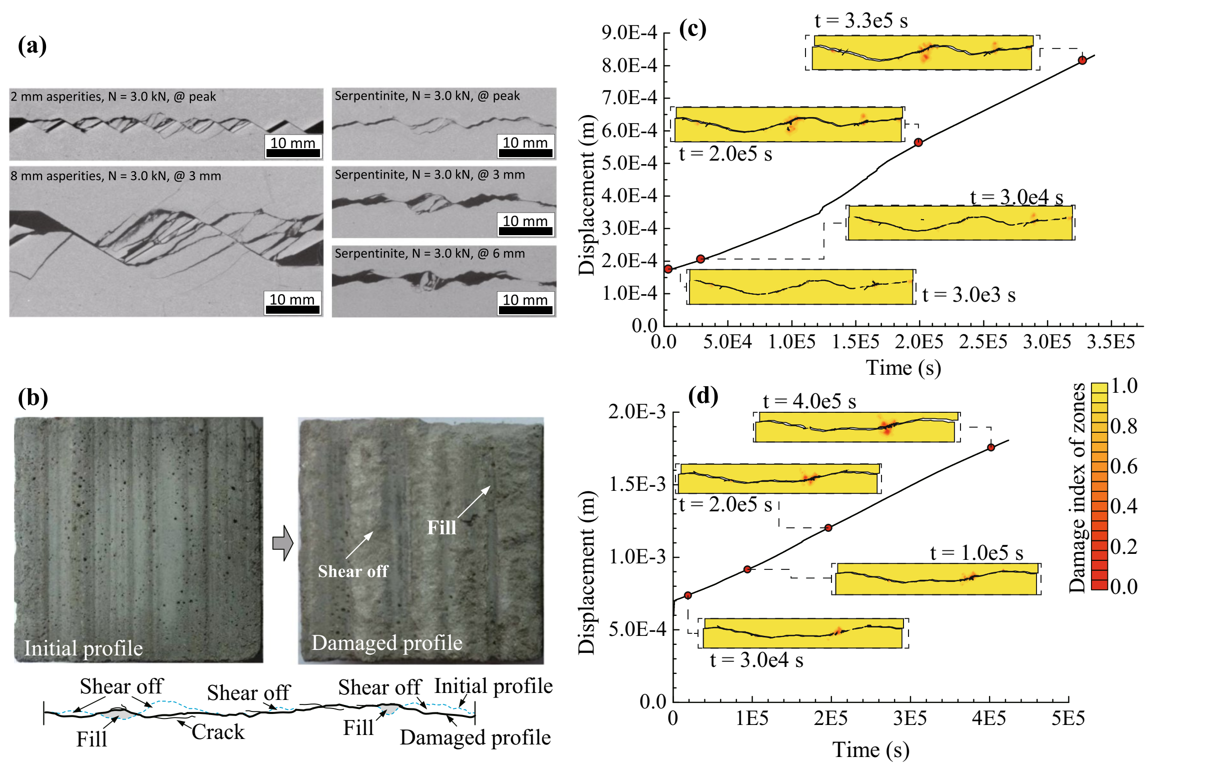

Fig. 15 Asperity destruction observed in shear experiments. (**a**) Asperity damage occurred in static shear test (Tatone 2014). (**b**) Roughness damage due to static fatigue under shear, after Wang (2017a). (**c**) Damage index contours in creep simulation for joint with $JRC = 15$, $\sigma_n = 4$ MPa, and $\tau/\tau_S = 0.95$. (**d**) Damage index contours in creep simulation for joint with $JRC = 11$, $\sigma_n = 4$ MPa, and $\tau/\tau_S = 0.95$

$$\sigma_n^I > \sigma_n^{II}, \tag{9}$$

then the long-term shear strength ratio of case I, which is referred as ξ^I, can be obtained from

$$\xi^I = \frac{\left(JRC - JRC_{c-mob}\right)\log\left(\frac{JCS}{\sigma_n^I}\right) + \phi_b}{JRC\log\left(\frac{JCS}{\sigma_n^I}\right) + \phi_b}. \tag{10}$$

For case II, the ξ^{II} value can be calculated similarly. Finally, according to Eqs. (5), (9) and (10), we have

$$\xi^I > \xi^{II}, \tag{11}$$

which means that the higher the normal stress is, the higher the long-term shear strength ratio ξ will be.

The analysis above presents a message that normal stress has more influence on the long-term stability of joints than roughness. For two joints with different roughness, they both may have lower long-term strengths if the rougher joint is loaded at a lower normal stress. For example, the long-term shear strengths are around 2.8 MPa for the joint models with $JRC = 19$, $\sigma_n = 2$ MPa, $JRC = 3$, $\sigma_n = 4$ MPa (Fig. 11). A higher normal stress increases not only the long-term shear stress but also the long-term shear stress ratio (Figs. 12 and 13). Thus, a sufficiently high normal stress is needed to enable the asperities of rough joints to resist creep slipping under shear.

4.2 Creep Deformation of Joints

Three creep stages, i.e., initial, secondary and tertiary creeps, are commonly observed in creep experiment of rock. However, both experimental test and numerical simulation results (Figs. 9 and 10) reveal that the creep deformation of rock joints is very different from that of rock. A joint will slip at a relatively constant velocity if the applied shear stress is beyond its long-term shear strength. The higher the applied shear stress is, the larger the sliding velocity will be.

The sliding velocities obtained from the creep simulation are summarized in Table 2. For strain curves shown Fig. 10a, b, d, the sliding velocities, which are estimated using the average value from 0 to 1.5e5 s, are relatively stable. For the strain curves shown Fig. 10c, the sliding velocities are calculated using the part of the strain curves from 6.0e4 to 8.0e4 s.

It is seen that the shear loading ratio, the normal stress, and the *JRC* value all influence the sliding velocity. As shown in Fig. 16, for joint models that are loaded with the same shear loading ratio, the creep sliding velocity is negatively correlated with the applied normal stress (Fig. 16c, d) and positively correlated with the *JRC* value (Fig. 16a, b).

The variation of the sliding velocity tends to be related to the long-term shear strength ratio ξ. On the one hand, as mentioned in Sect. 4.1, a larger *JRC* will decrease the long-term shear strength ratio of the joint. A rougher joint tends to slid faster under the same stress loading ratio. On the other hand, a higher normal stress will increase the long-term shear strength ratio ξ significantly. The negative correlation between σ_n and the sliding velocity is observed under the same stress loading ratio.

It is concluded that compared with joint roughness, confinement (normal stress) is a more important factor that influences joint creep deformation. For a given rock mass structure, adding and preserving confinement can slow down creep deformations of discontinuities, thereby prolonging the lifetime of the structure.

In engineering design analysis, it is impractical to conduct grain-scale numerical analysis considering the details of joint surface profiles. In the next section, we propose a macroscopic creep slipping model for rock joints, which can be used to simulate joint creep deformation in conventional numerical models that consider joints a planar feature explicitly.

5 A Creep Slipping Model of Rock Joints

5.1 Creep Deformation Formulas

Based on the simulation results presented above, it is seen that joint roughness (*JRC*), shear loading ratio (τ/τ_S) and long-term shear strength ratio (ξ) are the three major factors that influence the sliding velocity of joint. Thus, a creep slipping model is proposed to estimate the sliding velocity, which is expressed as

$$\dot{\varepsilon} = \begin{cases} C_j \cdot \log(10 + JRC) \cdot \frac{\tau/\tau_S - \xi}{1 - \tau/\tau_S}, & \tau \geq \tau_L \\ 0, & \tau < \tau_L \end{cases} \tag{12}$$

where the $\dot{\varepsilon}$ is the shear strain rate (unit: h^{-1}) of joint (the shear strain is equal to shear displacement divided by the length of the joint), C_j is a dimensionless parameter which is used to balance the influence of loading rate (for both normal and shear stresses) (Tang and Wong 2016), rheological properties of rock, and filling materials (Malan 1998) on the shear strain rate. C_j can be expressed as $C_j = C_1 10^{C_2}$, and C_1 ranges from 1 to 10 and can be determined by fitting experimental data; C_2 is in the order of the tested creep strain rate of rock joints.

Figure 17 and Table 2 present the simulation results and the predicted value of $\dot{\varepsilon}$ using Eq. (12). In Fig. 17, each point represents different simulation cases with different

Table 2 Loading condition and simulated deformation features of grain-scale models

JRC	σ_n (MPa)	τ_S (MPa)	ϕ (°)	τ/τ_S	τ (MPa)	Simulated ξ	Simulated $\dot{\varepsilon}$ (h^{-1})	*Predicted ξ	*Predicted $\dot{\varepsilon}$ (h^{-1})
3	2.00	1.63	39.15	0.80	1.30	0.85	–	0.89	–
			39.15	0.90	1.47		9.00e-6		1.37e-5
			39.15	0.95	1.55		2.50e-5		3.87e-5
	4.00	2.88	35.75	0.90	2.59	0.91	–	0.97	–
			35.75	0.93	2.66		3.60e-6		9.13e-6
			35.75	0.95	2.74		2.74e-5		2.37e-5
	8.00	5.16	32.85	0.95	4.91	0.97	–	0.99	–
			32.85	0.98	5.06		1.98e-4		3.75e-5
7	2.00	2.23	48.06	0.70	1.56	0.75	–	0.71	–
			48.06	0.80	1.78		1.80e-5		7.57e-6
			48.06	0.90	2.00		4.44e-5		2.62e-5
			48.06	0.95	2.11		5.22e-5		6.05e-5
	4.00	3.78	43.35	0.80	3.02	0.85	–	0.89	–
			43.35	0.90	3.40		7.92e-5		1.51e-5
			43.35	0.95	3.59		5.63e-5		4.28e-5
	8.00	6.40	38.64	0.95	6.08	0.97	–	0.97	–
			38.64	0.98	6.27		6.66e-5		4.14e-5
11	2.00	3.06	56.86	0.80	2.45	0.85	–	0.62	–
			56.86	0.90	2.76		5.40e-5		1.63e-5
			56.86	0.95	2.91		6.99e-5		4.60e-5
	4.00	4.69	49.55	0.90	4.22	0.93	–	0.80	–
			49.55	0.95	4.46		7.20e-5		2.30e-5
	8.00	7.71	43.94	0.95	7.32	0.97	–	0.94	–
			43.94	0.98	7.56		3.24e-5		4.45e-5
15	2.00	4.28	64.97	0.55	2.36	0.58	–	0.58	–
			64.97	0.60	2.57		6.30e-6		3.04e-6
			64.97	0.70	3.00		1.53e-5		9.06e-6
			64.97	0.80	3.43		2.34e-5		1.82e-5
			64.97	0.90	3.85		2.64e-5		4.38e-5
	4.00	6.12	56.85	0.80	4.90	0.85	–	0.73	–
			56.85	0.90	5.51		2.88e-5		1.72e-5
			56.85	0.95	5.82		8.28e-5		4.86e-5
	8.00	10.07	51.54	0.88	8.86	0.89	–	0.90	–
			51.54	0.90	9.06		9.60e-6		7.69e-6
			51.54	0.95	9.57		2.83e-5		3.77e-5
			51.54	0.98	9.87		4.32e-5		1.15e-4
19	2.00	5.07	68.47	0.50	2.54	0.55	–	0.55	–
			68.47	0.60	3.04		7.20e-6		4.50e-6
			68.47	0.70	3.55		1.68e-5		1.04e-5
			68.47	0.80	4.06		3.26e-5		2.01e-5
			68.47	0.90	4.56		4.44e-5		4.76e-5
	4.00	7.65	62.40	0.70	5.36	0.75	–	0.68	–
			62.40	0.80	6.12		1.78e-5		8.99e-6
			62.40	0.90	6.89		4.68e-5		3.12e-5
	8.00	12.43	57.23	0.90	11.19	0.93	–	0.87	–
			57.23	0.95	11.81		5.18e-5		2.54e-5

*Predicted values are calculated using Eqs. (12) and (13)

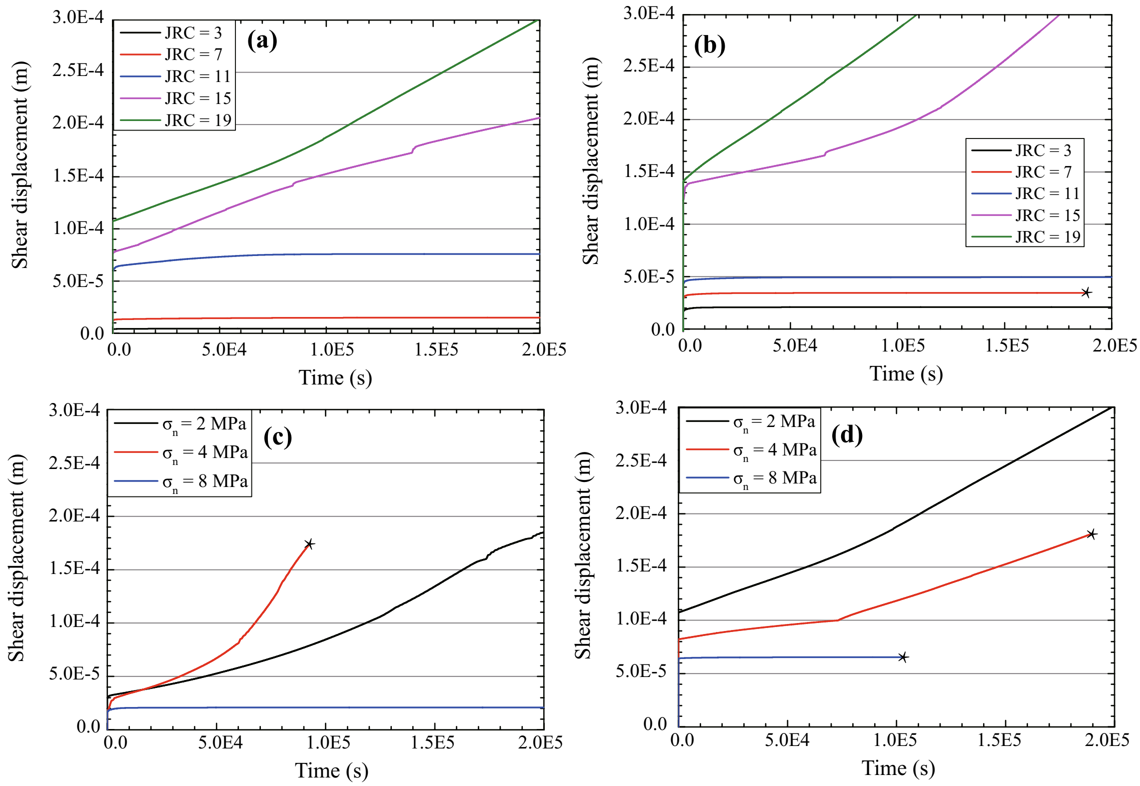

Fig. 16 Creep strain curves of joints under the same loading stress ratio. (**a**) Joints with different roughness for σ_n=2 MPa, τ/τ_S=0.8. (**b**) Joints with different roughness for σ_n=8 MPa, τ/τ_S=0.95. (**c**) Joint with *JRC*=3, τ/τ_S=0.95. (**d**) Joint with *JRC*=19, τ/τ_S=0.8. *Means that the simulation is stopped by user

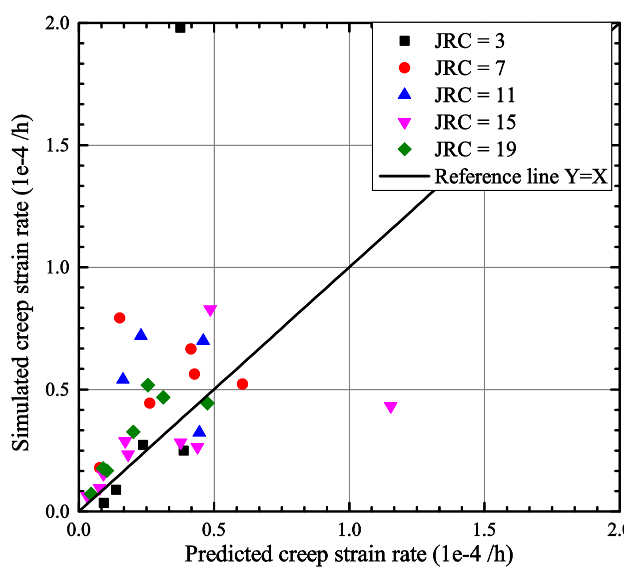

Fig. 17 Simulated vs. predicted results of creep strain rates

input parameters (i.e., *JRC*, normal stress and shear loading ratio), in which the x-axis represents the predicted results using Eq. (12) (where C_j is equal to 5.5e-6) and the y-axis represents the simulated results using the grain-scale joint model. A line $y=x$ is drawn as a reference. If the data points are closer to the reference line, it means that the predicted $\dot{\varepsilon}$ agrees well with the simulated result.

In addition to the validation using the simulation results of the grain-scale joint models, we also use published data to validate the proposed model (Eq. (12)). We tried our best to collect all available shear creep test data of rock joint from published literatures. Key information including short-term shear strength, *JRC* value, normal stress, shear loading ratio, sliding velocity and long-term shear strength ratio are listed in Table 3. These data are used to validate Eq. (12). As shown in Fig. 18, the x-axis presents the predicted results using Eq. (12), while the y-axis presents the experimental data. Data from the six datasets distribute near the reference line $y=x$, indicating that the proposed equation is able to predict the creep sliding velocity of joints well.

The long-term shear strength ratio ξ is one of the input parameters for calculating the creep strain rate using Eq. (12). As mentioned above, ξ is not a material constant, and it changes with joint roughness and normal stress. Thus, Eq. (13), which is an empirical equation fitted using the numerical simulation results, is presented to estimate the long-term shear strength ratio ξ of joints.

Table 3 Test conditions and experimental creep test results

UCS (MPa)	*JRC*	σ_n (MPa)	τ_S (MPa)	τ/τ_S	τ (MPa)	ξ	Tested $\dot{\varepsilon}$ (h^{-1})	*Predicted $\dot{\varepsilon}$ (h^{-1})	**Fitted C_j	References
21.7	1	2.17	1.76	0.80	1.41	0.79	7.00e-7	1.82e-7	3.5e-7	(Wang et al. 2017a)
				0.90	1.58		2.25e-6	1.21e-6		
		4.34	3.89	0.80	3.11	0.81	1.30e-6	1.82e-7		
				0.90	3.50		1.45e-6	1.09e-6		
		6.51	4.73	0.80	3.78	0.79	1.17e-6	1.82e-7		
				0.90	4.26		1.65e-6	1.21e-6		
	7	2.17	2.20	0.80	1.76	0.82	1.00e-6	3.05e-7		
				0.90	1.98		1.10e-6	1.22e-6		
		4.34	4.54	0.80	3.63	0.77	4.50e-7	3.73e-7		
				0.90	4.09		1.36e-6	1.55e-6		
		6.51	5.31	0.80	4.25	0.80	3.00e-7	0.00e0		
				0.90	4.78		1.04e-6	1.36e-6		
	19	2.17	3.58	0.80	2.86	0.78	1.10e-6	3.62e-7		
				0.90	3.22		2.50e-6	1.77e-6		
		4.34	6.26	0.80	5.01	0.73	1.22e-6	6.77e-7		
				0.90	5.63		1.19e-6	2.11e-6		
		6.51	7.90	0.70	5.53	0.71	6.00e-7	1.71e-7		
				0.80	6.32		8.50e-7	7.68e-7		
				0.90	7.11		1.20e-6	2.23e-6		
190.0	4.8	0.20	0.11	0.99	0.10	0.85	1.51e-6	1.37e-6	3.5e-8	(He et al. 2019)
		0.40	0.20	0.99	0.20	0.85	2.17e-6	2.19e-6		
		0.60	0.30	1.00	0.30	0.86	2.98e-6	3.07e-6		
100.0	18	5.00	12.84	0.70	8.98	0.56	3.03e-7	5.95e-7	3.3e-7	(Zhang et al. 2012)
				0.89	11.37		1.65e-6	2.39e-6		
		12.50	22.33	0.56	12.58	0.52	6.40e-7	2.28e-7		
				0.67	14.88		7.96e-7	5.48e-7		
				0.77	17.28		1.99e-6	1.07e-6		
		15.00	25.50	0.59	14.97	0.52	7.58e-7	3.00e-7		
				0.66	16.88		1.73e-6	5.33e-7		
436.0	2	0.50	0.28	0.53	0.15	0.53	1.85e-7	4.55e-8	3.6e-7	(Malan 1998)
				0.63	0.17		2.97e-7	3.30e-7		
				0.76	0.21		5.96e-7	7.53e-7		
				0.84	0.23		8.92e-7	1.38e-6		
				0.90	0.25		1.28e-6	2.37e-6		
		1.00	0.53	0.58	0.31	0.58	7.87e-7	5.56e-8		
				0.73	0.39		9.91e-7	5.75e-7		
				0.89	0.47		2.07e-6	1.87e-6		
		1.50	0.82	0.37	0.30	0.37	4.93e-7	1.79e-8		
				0.51	0.42		6.83e-7	2.99e-7		
				0.66	0.54		1.06e-6	6.20e-7		
				0.78	0.64		1.86e-6	1.14e-6		
				0.87	0.72		2.26e-6	2.15e-6		
				0.93	0.77		4.70e-6	4.29e-6		
21.7	19	4.35	6.26	0.80	5.01	0.73	4.30e-5	1.93e-5	1.0e-5	(Wang et al. 2017b)
				0.90	5.63		7.40e-5	6.03e-5		
				0.93	5.82		9.20e-5	9.34e-5		

*Predicted values are calculated using Eq. (12)

**Model parameter of Eq. (12) used in each cases

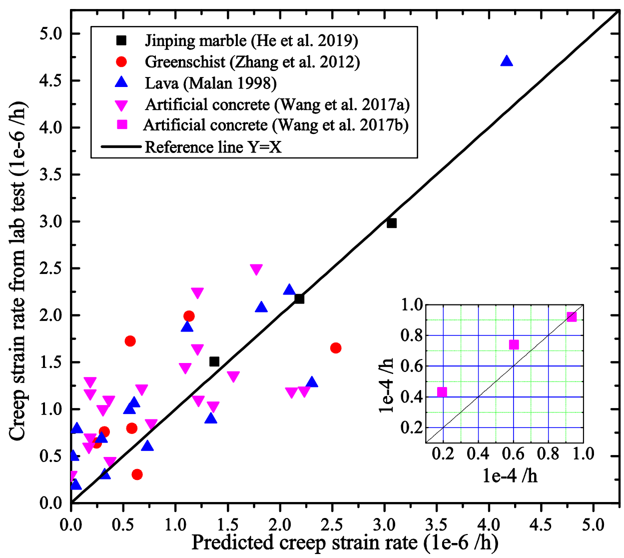

Fig. 18 Experimental tested vs. predicted creep strain rates. One set of data from Wang (2017b) is located at 1e-5 h^{-1}, which is shown in the insert

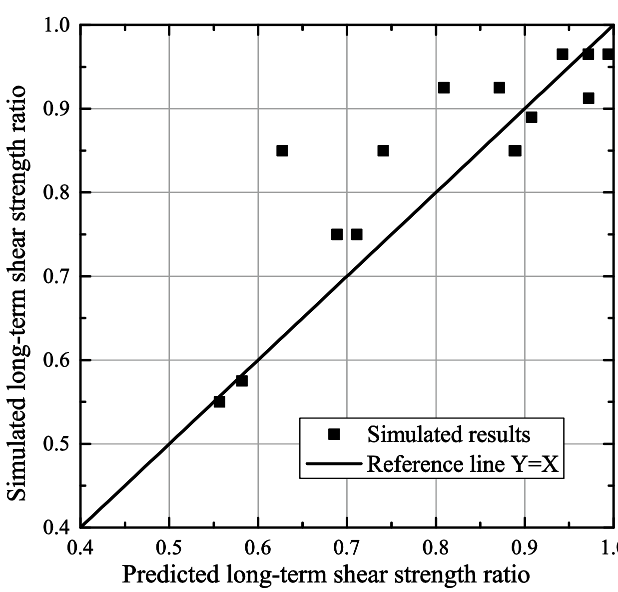

Fig. 19 Simulated vs. predicted long-term shear strength ratios

$$\xi = 1 - \frac{1 - \xi_0}{\left(10^4 \cdot \left(\frac{\sigma_n}{JCS}\right)^{1.5} \Big/ JRC^{1.2}\right) + 1}, \tag{13}$$

where the basic long-term shear strength ratio ξ_0 is a constant, which is influenced by the rheological properties of rock. The ξ_0 value is equal to 0.5 for the grain-scale joint models.

The numerically simulated and the equation-predicted (using Eq. (13)) ξ values are presented in Fig. 19, showing a relatively good agreement between the two. Because the published data of long-term shear strength ratios are limited, there are not enough experiment data available to further verify Eq. (13). Hence, if Eq. (13) is used to estimate the long-term shear strength ratio ξ of joints of other rock types, it is suggested that some laboratory tests or filed measurements be conducted to determine the ξ_0 value and further verify Eq. (13).

5.2 Model Implementation for Simplified Flat Joints

The grain-scale models perform well in simulating the creep behavior of rock joints. However, in numerical simulation it is unrealistic to build grain-scale models for all joints in large-scale rock structures. Thus, a creep constitutive model for simplified flat joints is needed. According to literatures, the creep strain curves of rock joints are usually fitted using Burgers model (Xu and Yang 2005; Yang et al. 2013, 2007; Zhang et al. 2015, 2016); however, the four model parameters of Burgers model not only are affected by normal stress and joint roughness, but also are shear stress dependent. This is different from the Burgers creep model of intact rock, in which all four model parameters are stress independent. This means that when the shear stress is changed, the model parameters will not be valid anymore. Therefore, Burgers model cannot be directly used as a creep constitutive model for rock joints.

On the other hand, Eqs. (12) and (13), in which the model parameter C_j and the constant ξ_0 are stress independent, can be adopted in a creep constitutive model to describe time-dependent deformation behaviors of rock joints.

In the creep fatigue process, damages that occur on the asperities of grain-scale joint models are observed (Fig. 15c and d), which result in the reduction of joint roughness. For a simplified flat joint, the strength degradation method is adopted to mimic the roughness destruction under creep loading conditions. A roughness degradation model is proposed and shown in Fig. 20, which can be used to model short- and long-term strengths and time-dependent deformations of flat joints. The short-term shear strength is determined by the Barton's non-linear strength criterion, and the long-term shear strength is calculated using the short-term shear strength and Eq. (13). When the shear stress is beyond the long-term shear strength, the joint roughness (*JRC*) will be degraded which will result in slip deformation between joint walls. The sliding velocity is controlled by Eq. (12). When the shear stress or the normal stress is changed, the long-term strength and the sliding velocity will be adjusted accordingly.

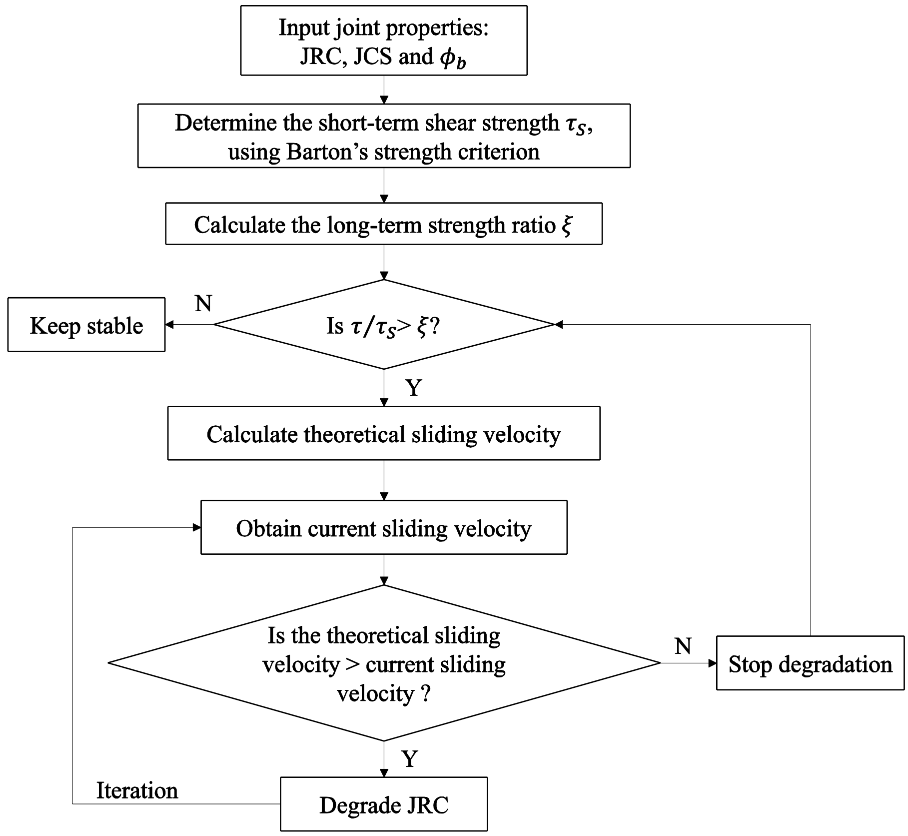

Fig. 20 Flowchart of creep slipping model for flat joint in UDEC

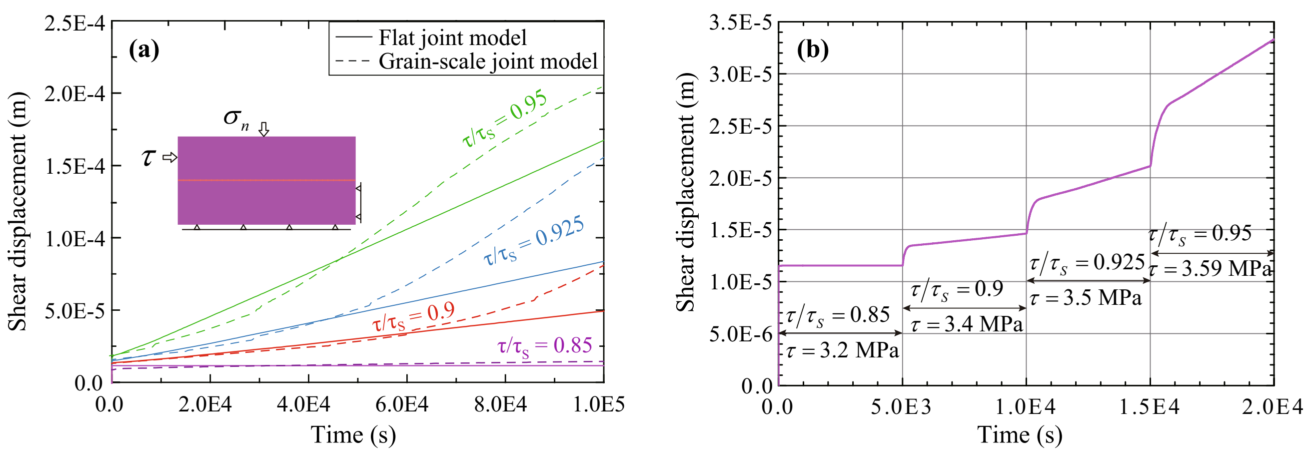

Fig. 21 Creep deformation of a macroscopically flat joint under different shear loading ratios (for $JRC = 7$, $\sigma_n = 4$ MPa). (**a**) Creep curves of joint under constant shear stress. (**b**) Creep curves of joint under variable shear loadings

The creep slipping model performs well in controlling the creep behavior of simplified flat joints. As shown in Fig. 21, the creep deformation of a flat joint is simulated using a shear model with a length of 10 cm and a height of 5 cm in UDEC. The short- and long-term shear strengths and creep deformation of the flat joint are controlled by the creep slipping model of rock joints, without being affected by the mechanical properties of the rock of the joint walls. For the flat joint with input parameters of $JRC = 7$, $\sigma_n = 4$ MPa, the long-term strength ratio ξ is 0.89 according to Eq. (13), and creep slipping occurs when $\tau/\tau_S > \xi$. As shown in Fig. 21a, when $\tau/\tau_S = 0.85$, which is smaller than 0.89, there is no sliding velocity captured after 100 s. For the rest of the three cases with $\tau/\tau_S > 0.89$, creep sliping is observed. The sliding velocity is controlled by Eq. (12). The creep strain curves of the grain-scale models are presented in Fig. 21a. The creep deformations of the grain-scale joint model after 100 s of each case are presented and compared with those of the flat joint models. The initial shear displacement of the grain-scale joint model is influenced by the roughness profile of the joint. Even though joint roughness profile is not explicitly considered in the simplified creep slipping model, the model captures the shear displacement well.

Because the model parameters of Eq. (12) are all stress-independent, the creep deformation of flat joints can be controlled under variable shear loading conditions (Fig. 21b). When the shear loading ratio is increased from 0.85 to 0.95, the sliding velocity of the joint increases in a manner that follows the theoretical value determined from Eq. (12).

6 Discussion

The creep strain rate of joints obtained from the simulation results is in the order of 1e-5 h^{-1} (Fig. 17). Most of the published experiment data show creep strain rates about 1e-6 h^{-1}, but one set of data from Wang (2017b) is located at 1e-5 h^{-1} (Fig. 18). The large difference among the datasets is probably attributed to the variation of the rheological properties of rock types, the different loading rates (both normal and shear loadings) (Tang and Wong 2016), and the difference among the creep testing machines. This is why model parameter C_j in Eq. (12) is needed to balance the influence of these factors through parameter calibration. However, for the same dataset using the same rock type and under the same test condition, the influence of σ_n, τ/τ_S and *JRC* on the creep deformation (i.e., long-term shear strength and sliding velocity) can be described properly using Eqs. (12) and (13), as shown in Figs. 17 and 18.

One thing that needs to be mentioned is the independence between the parameters in the fitting formulas of Eqs. (12) and (13). The three input parameters, σ_n, τ/τ_S and *JRC*, are independent each other. σ_n is independent of *JRC*. Both σ_n and *JRC* affect the short-term shear strength τ_S, but the loading ratio τ/τ_S is independent of both σ_n and *JRC*.

The simulated creep deformations of joints using the grain-scale models agree well with the experimental data. First, the long-term shear strength and the relatively constant creep sliding velocity, which are important creep deformation characteristics, are captured in the simulation and they agree well with the experimental data (Bowden and Curran 1984; Wang et al. 2017b; Yang et al. 2007). Second, the asperity destruction is captured in the simulation, as illustrated in Fig. 15c, d. The roughness degradation method used in the creep model for the simplified flat joint performs well in mimicking the time-dependent strength and creep deformation of joints, which verifies the finding of Liu et al. (2019) who state that the asperity degradation governs the time-dependent deformation behavior of joint under shear. Thirdly, the importance of normal stress is confirmed. The modeling results agree with the experimental results of granite discontinuities (Gadi 1986), which state the creep deformations of joints are very different under different normal stress conditions. It explains that a higher confinement is beneficial to improving the long-term stability of jointed rock mass.

The grain-based joint model is demonstrated to be a good model to simulate time-dependent deformation of joints. Because the creep deformation governed by the joint asperities is simulated at the grain scale, it provides a novel approach to study the creep mechanism of rock joints. For simplified flat joints, the proposed creep slipping model can simulate the long-term strength and creep slipping velocity well. This makes it possible to consider creep deformation of rock joints when simulating time-dependent deformation of jointed rock mass, in which the creep deformation of joint plays an important role.

However, the limitation of this creep slipping model should also be mentioned. The creep slipping model considers only the strength degradation due to stress erosion of the joint asperities. Water seepage and weathering of rock joints during creep deformation are not considered. The empirical Eqs. (12) and (13) are fitted from the experimental data and the simulation results using the grain-scale joint models. Uncertainties associated with these two formulas may be due to the limited amount of usable experimental data from publication and the uncertainty coming from the grain shape and size because the Voronoi tessellation generator in UDEC is used to model the geometry of mineral grains in the GBM-TtoF models.

7 Conclusion

This article investigates the creep deformation of unweathered clean rock joints. Firstly, five grain-scale joint models are established using the GBM-TtoF creep model to simulate the creep deformation of rock joints with realistic surface roughness. Then, creep slipping equations, which are fitted by the simulation results and verified using experimental data, are presented. Finally, a creep slipping model for simplified flat joints is developed using the creep slipping equations.

The grain-scale joint models perform well in simulating the creep deformation of rock joints. Using the calibrated GBM-TtoF creep models, time-dependent joint deformations governed by stress erosion of joint asperities can be simulated. In this manner, the long-term shear strength and the creep slipping of rock joint can be simulated.

Normal stress is more important than roughness to improve long-term stability of rock joints. For a rough joint under creep shear loading, a high normal stress is beneficial to improving the long-term strength of the joint. This means that providing confinement to jointed rock masses through rock support is important to ensure longer stability of the rock masses.

It is impractical to conduct grain-scale numerical analysis considering detailed joint surface profiles in engineering design analyses. The proposed creep slipping model captures well the long-term strength and creep slipping velocities of flat joints under both constant and variable shear loading conditions. It can be used to simulate time-dependent deformation of jointed rock mass using DEM by considering flat joints in the models.

Acknowledgements This work was financially supported by NSERC (Natural Science and Engineering Research Council of Canada, RGPIN-2016-04052), the China Scholarship Council (Grant No. CSC201806370225), and MIRARCO of Laurentian University.

Compliance with Ethical Standards

Conflict of interest The authors wish to confirm that there are no known conflicts of interest associated with this publication and there has been no significant financial support for this work that could have influenced its outcome.

References

Alejano LR, González J, Muralha J (2012) Comparison of different techniques of tilt testing and basic friction angle variability assessment. Rock Mech Rock Eng 45:1023–1035

Bahaaddini M, Hagan P, Mitra R, Khosravi M (2016) Experimental and numerical study of asperity degradation in the direct shear test. Eng Geol 204:41–52

Bandis S, Lumsden A, Barton N (1981) Experimental studies of scale effects on the shear behaviour of rock joints. In: Int J Rock Mech Mining Sci Geomech Abstr, 1981. vol 1. Elsevier, pp 1–21

Barton N (1995) The influence of joint properties in modelling jointed rock masses. In: 8th ISRM Congress, 1995. International Society for Rock Mechanics and Rock Engineering

Barton N, Choubey V (1977) The shear strength of rock joints in theory and practice. Rock Mech 10:1–54

Barton N, Bandis S, Bakhtar K (1985) Strength, deformation and conductivity coupling of rock joints. In: Int J Rock Mech Mining Sci Geomech Abstr, 1985. vol 3. Elsevier, pp 121–140

Bhasin R, Høeg K (1998) Parametric study for a large cavern in jointed rock using a distinct element model (UDEC-BB). Int J Rock Mech Min Sci 35:17–29

Bieniawski Z (1976) Rock mass classification in rock engineering applications. In: Proceedings of a Symposium on Exploration for Rock Engineering, 1976, 1976. pp 97–106

Bieniawski ZT (1989) Engineering rock mass classifications: a complete manual for engineers and geologists in mining, civil, and petroleum engineering. Wiley, Hoboken

Boon CW (2013) Distinct element modelling of jointed rock masses: algorithms and their verification., Oxford University, UK

Bowden RK, Curran J (1984) Time-dependent behaviour of joints in Shale. In: The 25th US Symposium on Rock Mechanics (USRMS), 1984. American Rock Mechanics Association

Chen WZ, Zhu WS, Shao JF (2004) Damage coupled time-dependent model of a jointed rock mass and application to large underground cavern excavation. Int J Rock Mech Min Sci 4:669–677

Chigira M (1992) Long-term gravitational deformation of rocks by mass rock creep. Eng Geol 32:157–184

Cristescu N, Fotă D, Medveş E (1987) Tunnel support analysis incorporating rock creep. In: Int J Rock Mech Mining Sci Geomech Abstr, 1987. vol 6. Elsevier, pp 321–330

Feng J, Chuhan Z, Gang W, Guanglun W (2003) Creep modeling in excavation analysis of a high rock slope. J Geotech Geoenviron Eng 129:849–857

Gadi AM (1986) Creep along a discontinuity in granite.

Glamheden R, Hoekmark H (2010) Creep in jointed rock masses. State of knowledge. Swedish Nuclear Fuel and Waste Management Co

Goodman RE (1989) Introduction to rock mechanics, vol 2. Wiley, New York

He ZL, Zhu ZD, Ni XH, Zj Li (2019) Shear creep tests and creep constitutive model of marble with structural plane. Eur J Environ Civil Eng 23:1275–1293

Itasca (2015) UDEC, Universal distinct element code., 6.0 edn. Itasca Consulting Group. Inc, Minneapolis

Kemeny J (2003) The time-dependent reduction of sliding cohesion due to rock bridges along discontinuities: a fracture mechanics approach. Rock Mech Rock Eng 36:27–38. https://doi.org/10.1007/s00603-002-0032-2

Lajtai E (1991) Time-dependent behaviour of the rock mass. Geotech Geol Eng 9:109–124

Lajtai E, Gadi A (1989) Friction on a granite to granite interface. Rock Mech Rock Eng 22:25–49

Liu G, Cai M (2020) Modeling time-dependent deformation behavior of brittle rock using grain-based stress corrosion method. Comput Geotech 118:103323

Liu J, Feng XT, Ding XL, Zhou HM In situ tests on creep behavior of rock mass with joint or shearing zone in foundation of large-scale hydroelectric projects. In: Key Engineering Materials, 2004. Trans Tech Publ, pp 1097–1102

Liu A, Lin WL, Jiang JC (2019) Investigation of the long-term strength properties of a discontinuity by shear relaxation tests. Rock Mechanics and Rock Engineering, pp 1–10

Malan D (1998) An investigation into the identification and modeling of time-dependent behaviour of deep level excavations in hard rock [Ph. D. Thesis]. South Africa: University of Witwatersrand

Martín LB, Rutqvist J, Birkholzer JT (2015) Long-term modeling of the thermal–hydraulic–mechanical response of a generic salt repository for heat-generating nuclear waste. Eng Geol 193:198–211

Potyondy DO (2007) Simulating stress corrosion with a bonded-particle model for rock. Int J Rock Mech Mining Sci 44:677–691

Schmidtke RH, Lajtai E The long-term strength of Lac du Bonnet granite. In: Int J Rock Mech Mining Sci Geomech Abstr, 1985. vol 6. Elsevier, pp 461–465

Shen MR, Zhang QZ (2010) Study of shear creep characteristics of greenschist discontinuities. Chin J Rock Mech Eng 29:1149–1155

Shrader-Frechette KS (1993) Burying uncertainty: Risk and the case against geological disposal of nuclear waste. Univ of California Press,

Tang ZC, Wong LNY (2016) Influences of normal loading rate and shear velocity on the shear behavior of artificial rock joints. Rock Mech Rock Eng 49:2165–2172

Tatone BSA (2014) Investigating the evolution of rock discontinuity asperity degradation and void space morphology under direct shear. University of Toronto, Canada
Wang MZ, Cai M (2020) A grain-based time-to-failure creep model for brittle rocks. Comput Geotech. https://doi.org/10.1016/j.compgeo.2019.103344
Wang JA, Wang YX, Cao QJ, Ju Y, Mao LT (2015) Behavior of microcontacts in rock joints under direct shear creep loading. Int J Rock Mech Min Sci 78:217–229
Wang Z, Shen MR, Ding WQ, Jang B, Zhang QZ (2017a) Time-dependent behavior of rough discontinuities under shearing conditions. J Geophys Eng 15:51–61
Wang Z, Shen MR, Tian GH, Zhang QZ (2017b) Time-dependent strength of rock mass discontinuity with different values of JRC. Chin J Rock Mechan Eng 31:10. https://doi.org/10.13722/j.cnki.jrme.2016.0018
Wasantha P, Ranjith P, Zhang Q, Xu T (2015) Do joint geometrical properties influence the fracturing behaviour of jointed rock? An investigation through joint orientation. Geomech Geophys Geo-Energy Geo-Resour 1:3–14
Xu WY, Yang SQ (2005) Experiment and modeling investigation on shear rheological property of joint rock. Chin J Rock Mechan Eng 24:5536–5542
Xu T, Xu Q, Tang CA, Ranjith P (2013) The evolution of rock failure with discontinuities due to shear creep. Acta Geotech 8:567–581
Xue YT, Mishra B Numerical Study on the Time-Dependent Behavior of Rock Joints. In: 53rd US Rock Mechanics/Geomechanics Symposium, 2019. American Rock Mechanics Association
Yang SQ, Xu WY, Yang SL (2007) Investigation on shear rheological mechanical properties of shale in Longtan Hydropower Project. Yantu Lixue (Rock and Soil Mechanics) 28:895–902
Yang B, Mo S, Wu P, He C (2013) An empirical constitutive correlation for regular jugged discontinuity of rock surfaces. Adv Appl Math Mech 5:258–268
Zhang X-P, Wong LNY (2013) Crack initiation, propagation and coalescence in rock-like material containing two flaws: a numerical study based on bonded-particle model approach. Rock Mech Rock Eng 46:1001–1021
Zhang Q, Shen M, Ding W (2012) Study of shear creep constitutive model of greenschist structural plane. Rock Soil Mech 33:7. https://doi.org/10.16285/j.rsm.2012.12.009
Zhang QZ, Shen MR, Ding WQ (2015) The shear creep characteristics of a green schist weak structural marble surface. Mech Adv Mater Struct 22:697–704
Zhang QZ, Shen MR, Jang BA, Ding WQ (2016) Creep behavior of rocks with rough surfaces. J Mater Civ Eng 28:04016063
Zhang QZ, Wu CZ, Fei XC, Jang BA, Liu DQ (2019) Time-dependent behavior of rock joints considering asperity degradation. J Struct Geol 121:1–9